Infrared spectroscopy of carbo-ions. IV. The $A\,^2\Pi_u$–$X\,^2\Sigma_g^+$ electronic transition of C_2^-

Brent D. Rehfuss, Di-Jia Liu,[a] Bianca M. Dinelli,[b] Mary-Frances Jagod, Wing C. Ho, Mark W. Crofton,[c] and Takeshi Oka

Department of Chemistry and Department of Astronomy and Astrophysics, The University of Chicago, Chicago, Illinois 60637

(Received 19 January 1988, accepted 24 March 1988)

The infrared spectrum of the $A\,^2\Pi_u \leftarrow X\,^2\Sigma_g^+$ electronic transition of C_2^- has been observed under high resolution and analyzed. Three bands $(v' \leftarrow v) = (0,0)$, $(1,1)$ and $(0,1)$ have been observed; the first two bands were observed by using the difference laser frequency system in the frequency range of 3960–3780 cm^{-1} and the last by using a diode laser in the frequency range of 2210–2120 cm^{-1}. A gas mixture of 50 mTorr of acetylene and 7 Torr of He was used for the ac discharge in an air-cooled and a water-cooled multiple inlet–outlet discharge tube. The simplicity of the optimum gas mixture suggested that C_2^- is produced directly by simple dissociative electron attachment of acetylene. Altogether 103 absorption lines have been observed and accurately measured. Most of them are P, Q, and R form branches of allowed $F_1 \leftrightarrow F_1$, $F_2 \leftrightarrow F_2$ transitions although some forbidden $F_1 \leftrightarrow F_2$ transitions and O and S transitions have also been measured. The hot bands $(1,1)$ and $(0,1)$ have been observed with intensity which is less than that for the $(0,0)$ by a factor of only 2 or 3, in spite of the fact that the Franck–Condon factors of these transitions are lower than that for the $(0,0)$ by 2.0 and 3.2, respectively, indicating that the vibrational temperature of C_2^- in the He plasma is extremely high. All observed transitions are simultaneously fit to the formula for a $^2\Pi_u \leftarrow {}^2\Sigma_g^+$ transition. The formulation of Brown and Watson has been used for the Hamiltonian for the $^2\Pi_u$ state. Molecular constants for C_2^- in the two electronic states have been determined from the least-squares fitting. The constants are compared with those of other species isoelectronic to C_2^-. A short discussion is given about the astrophysical implication of the spectrum.

I. INTRODUCTION

The diatomic carbon anion C_2^- is one of the very few gaseous molecular anions which have well bound electronic excited states. This special characteristic of C_2^- results from the high electronic affinity of C_2 and the low electronic excited states of C_2^-, both of which are due to the existence of the three low-lying terms ^3P, ^1D, and ^1S of carbon atoms. The special stability of C_2^- was first noted by Honig[1] in 1954 when he observed emission of neutral and charged carbon molecules from pure graphite filaments heated by arc up to 2600 K. He reported that the mass spectroscopic peak of C_2^- is "considerably stronger than the corresponding C_2^+ peak" and that the ratio of C_2^- to C_2 is $\sim 1/400$. From the variation of the C_2^- peak between temperatures of 2100–2400 K, Honig determined the electron affinity of C_2 to be 4.0 or 3.1 eV depending on the method of determination. Subsequently, the electron affinity of C_2 has been studied using dissociative electron attachment in C_2H_2 and C_2H_4 [$EA(C_2) \geqslant 2.9$ eV by von Trepke,[2] $EA(C_2) = 3.3 \pm 0.2$ eV by Locht and Momigny[3]] and photodetachment spectroscopy [$EA(C_2) = 3.54 \pm 0.05$ eV by Feldman[4]]. The most recent value is $3.374 \leqslant EA(C_2) \leqslant 3.408$ eV reported by Jones *et al.*[5] determined from their high resolution photodetachment spectroscopy of C_2.

C_2^- is isoelectronic to the series of 13-electron species CN, N_2^+, and CO^+, all of which have been well characterized through extensive studies of their optical spectra.[6,7] The lowest three energy levels for the four species are shown in Fig. 1. In 1968 Herzberg and Lagerqvist[8] attempted to observe absorption spectra of carbo-ions CH_4^+, CH_3^+, CH_2^+, and CH^+ in a flash discharge of methane, and instead observed new very simple Σ–Σ bands in the region 4800–6000 Å. They studied the bands extensively under high resolution and they provisionally assigned them to the $^2\Sigma_u^+ \leftarrow {}^2\Sigma_g^+$ transition of C_2^-. A year later Milligan and Jacox[9] concluded that a band system of carbon vapor trapped in inert gas matrices previously assigned[10] to C_2 were probably this same Σ–Σ transition of C_2^- since the intensity of the band increased in the presence of an electron donor such as atomic Cs. Other matrix isolation studies[11,12] followed giving more support to this interpretation. Finally, Lineberger and Patterson[13] conducted a two-photon photodetachment spectroscopy of C_2^- and showed conclusively that the Herzberg–Lagerqvist spectrum was indeed that of C_2^-. Further photodetachment studies by Jones *et al.* allowed them to probe high-lying autodetaching vibrational states of that electronic state. Hefter *et al.*[14] measured the autodetachment lifetimes of the high-lying B state.

[a] Present address: Department of Chemistry, University of California, Berkeley, California 94720.

[b] Present address: Instituto di Spettroscopia Molecolare, del C. N. R., Bologna, Italy 40126.

[c] Present address: Lawrence Livermore National Laboratory, Livermore, California 95440.

 0021-9606/88/130129-09$02.10

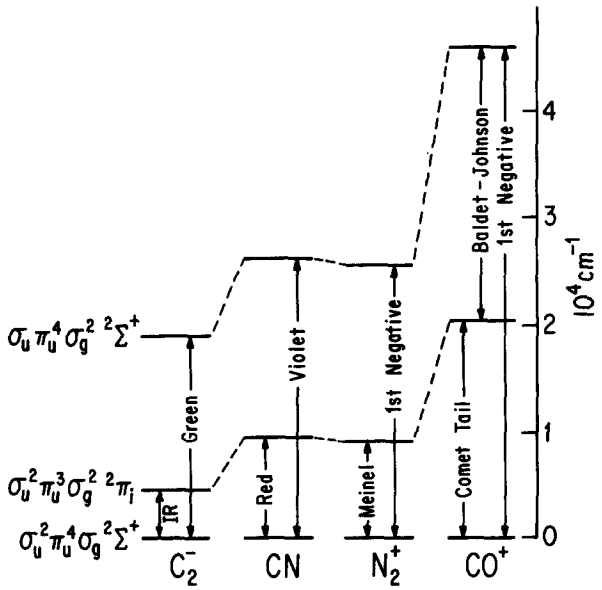

FIG. 1. Low-lying electronic energy levels, their electronic configurations, and the observed transitions of C_2^- and its isoelectronic species.

Numerous theoretical calculations[15–21] have predicted the low-lying $^2\Pi_u$ electronic state shown in Fig. 1, which is only about 1/2 eV above the ground state. Initial experimental evidence for this state was reported by Locht and Momigny[3] when they observed the second value of electron affinity $EA(C_2) = 2.2$ eV and attributed it to the appearance of C_2^- in the $A\ ^2\Pi_u$ state. More recently, Mead *et al.*[22] studied extensively the $B\ ^2\Sigma_u^+ \leftarrow X\ ^2\Sigma_g^+$ transition using a merged laser–ion beam spectrometer with sub-Doppler resolution. They noticed many significant perturbations of the B state by the $A\ ^2\Pi_u$ state and using deperturbation methods obtained the first spectroscopic information on the $A\ ^2\Pi_u$ state. They noted that a direct observation of the $A\ ^2\Pi_u$ state would be highly desirable. In the present paper we report our direct observation of the $A\ ^2\Pi_u^+ \leftarrow X\ ^2\Sigma_g^+$ transition in the infrared region. The approximate molecular term reported by Mead *et al.* provided a good guide for us as to which wavelength region to search for the spectrum. As noted later in this paper the constants reported by them are also close to more accurate values in this paper.

From the time that the hydrogen atom anion H^- was identified as the main species to cause the opacity of the Sun,[23,24] other negative ions have been considered in astrophysics as important sources of opacity in stars. Because of its simplicity and stability, C_2^- has been considered as one of the astrophysically important ions especially in carbon stars.[25,26] Wallerstein searched for the $B \leftarrow X$ visible transition in the hydrogen-poor carbon star HD 182040 without success,[27] while Vardya and Krishna Swamy advocate the use of the $A \leftarrow X$ infrared transitions for astronomical search and call for the laboratory studies on this ion.[28] It is our hope that the results presented in this paper not only give accurate quantum chemical information on this fundamental species but also lead to its detection in space.

II. EXPERIMENT

The experimental arrangement used in this paper is the same as that used previously for the spectroscopy of CH_3^+ (Refs. 29 and 30) and $C_2H_2^+$ (Ref. 31). Briefly, a difference frequency system developed by Pine[32] provides the frequency tunable infrared radiation and the velocity modulation technique developed by Gudeman and Saykally[33] is utilized to increase the sensitivity and to discriminate the ionic absorption from the stronger absorption due to a much more abundant neutral species. The velocity modulation method is particularly useful for negative ion spectroscopy because the opposite phase of the negative ion signals discriminates them from the more common signals of positive ions. This advantage has been clearly shown in the very recent activities of negative ion spectroscopy mainly in Saykally's laboratory including OH^- (Refs. 34–36), OD^- (Ref. 37), FHF^- (Ref. 38), NH_2^- (Ref. 39), SH^- (Ref. 40), N_3^- (Ref. 41), NCO^- (Ref. 42), NCS^- (Ref. 43), and HC_2^- (Ref. 44). These results also show that negative ions are produced in abundance in discharges.

The C_2^- ions were produced in a water-cooled ac discharge cell described previously.[30] The simple gas mixture of He and acetylene has been used; the acetylene concentration had to be kept very low to prevent rapid production of soot on the wall of the cell and thus discharge instability. The best results were obtained using a mixture of 50 mTorr of acetylene and 7 Torr of He. The addition of varied amounts of H_2 to the mixture did not increase the signal. Addition of CO_2 of various concentrations was also attempted without success due to the rapid carbon deposit buildup and instability of discharge. In the $He:C_2H_2$ gas mixture used for spectroscopy, absorptions of H_3^+ and CH_3^+ were not observed as expected from the lack of hydrogen in the discharge. The spectrum of $C_2H_2^+$ was weakly observed. The simplicity of the optimum discharge mixture suggests that C_2^- is produced directly by dissociative electron attachment:

$$C_2H_2 + e^- \rightarrow C_2^- + H + H\,. \qquad (1)$$

The hot band spectrum $A\ ^2\Pi_u(v=0) \leftarrow X\ ^2\Sigma_g^+(v=1)$ which appeared in the 4.6 μm region was observed using our diode laser spectrometer. The Spectra-Physics LS-3 infrared spectrometer was used using the same ac discharge as described above.

The spectral lines were measured using absorption of reference gases. For the $0 \leftarrow 1$ transition in the 4.6 μm region, spectra of OCS[45] and N_2O[46] have been used. For the measurement of the $0 \leftarrow 0$ and the $1 \leftarrow 1$ bands in the 2.5 μm region, the H_2O infrared spectrum[47] was used for the reference. The spectral lines of H_2O are sometimes widely spaced. We used the interference spike of a spectrum analyzer with free spectral range of 1500 MHz to interpolate between H_2O lines. The accuracy of frequency measurement is on the order of 0.003 cm^{-1} in general excepting for specially unfavorable cases where the reference spectral lines are spaced by more than a few cm^{-1}.

III. OBSERVED SPECTRUM

The three observed bands $0 \leftarrow 0$, $1 \leftarrow 1$, and $0 \leftarrow 1$ for the $A\ ^2\Pi_u \leftarrow X\ ^2\Sigma_g^+$ electronic transition are shown in Fig. 2 to-

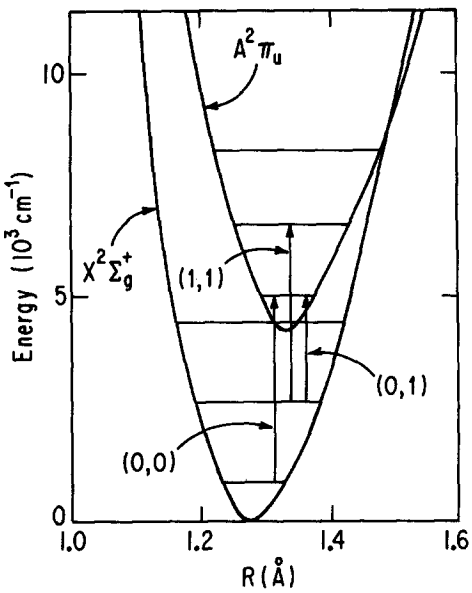

FIG. 2. Potential curves of C_2^- in low energy region and the three $A\,^2\Pi_u \leftarrow X\,^2\Sigma_g^+$ bands, $(v' \leftarrow v) = (0,0)$, (1,1), and (0,1), reported in this paper.

gether with the potential curves for the two electronic states. Initially the strongest $0 \leftarrow 0$ transitions were observed in the 2.5 μ region predicted by the work of Lineberger and his colleagues.[22] A typical trace of the spectrum is shown in Fig. 3. The large intensities of the signals are due to the large transition dipole moment of the electronic transition. Using the electronic transition dipole moment of 0.94 D predicted by Rosmus and Werner,[21] it is estimated that a C_2^- number concentration of the order of 10^8/cm^3 is sufficient to produce these spectral lines. The observed large intensities of these lines prompted us to also study the hot bands, $1 \leftarrow 1$ at the 2.6 μm region and $0 \leftarrow 1$ at the 4.6 μm region, both of which have been observed with good signal-to-noise ratios. A trace of the $1 \leftarrow 1$ band is shown in Fig. 3. According to the calculation of Mead *et al.*,[22] the Franck–Condon factors of the hot bands $1 \leftarrow 1$ and $0 \leftarrow 1$ transitions are smaller than that of the $0 \leftarrow 0$ transition by a factor of 2.0 and 3.2, respectively. The observation of these hot bands indicates a high vibrational temperature of C_2^- in the He plasma, which is estimated here to be $\gtrsim 5000$ K.

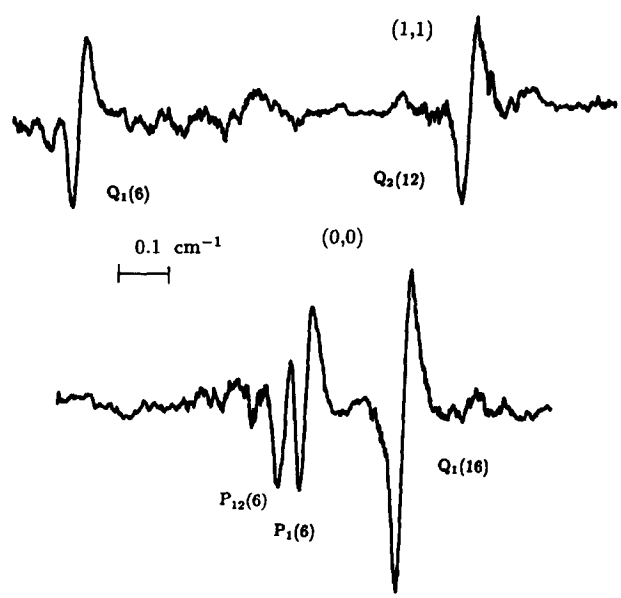

FIG. 3. Typical traces of the (0,0) band (lower trace) and the (1,1) band (upper trace) of the $A\,^2\Pi_u \leftarrow X\,^2\Sigma_g^+$ electronic transition of C_2^-. The weaker of the doublet in the lower trace is the $F_1 \leftarrow F_2$ transition which is forbidden for high J values [Hund case (b)] but is allowed for low J values [Hund case (a)]. The (1,1) band is weaker than the (0,0) band only by a factor of 2–3 (which is explained by the variation of the Franck–Condon factor) indicating that the vibrational temperature of C_2^- is extremely high.

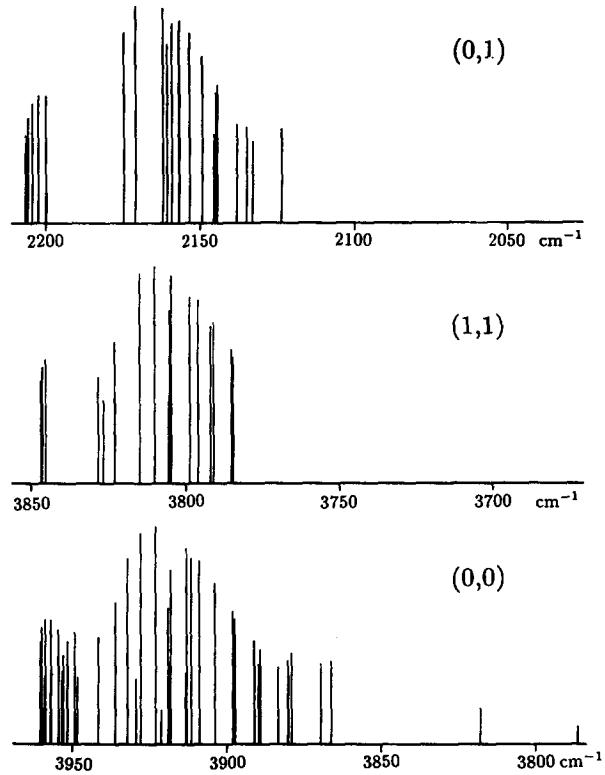

FIG. 4. Computer generated stick diagrams of the observed three bands. The R branch heads are clearly noted in the high frequency region. The central portion of the spectra are dominated by Q branch lines, and P branch lines tail off to low frequency region. Many lines were unobservable because of interference of the atmospheric water absorption lines.

Stick diagrams for the three observed bands are given in Fig. 4. They are typical $\Pi \leftarrow \Sigma$ perpendicular transitions with a lower B value in the upper state; the R branch lines form a sharp bandhead while P branch lines extend far to the lower frequencies and strongly pronounced Q branch lines appear at the center. Many spectral lines could not be observed because of interfering atmospheric water absorptions. The observed frequencies are summarized in Tables I–III.

IV. ANALYSIS OF THE SPECTRUM: THEORY

Since the initial theoretical work by Hill and Van Vleck[48] and Mulliken and Christy,[49] the Hamiltonian for $^2\Pi$ molecules has been discussed in many papers (see Refs. 50, 51, and 22 and references therein). We find the treatment of Brown and Watson[51,52] to be most transparent and use it for the analysis of our spectrum of C_2^-. The original rovibronic Hamiltonian operator related to rotation is written as

TABLE I. Transition frequencies of C_2^- (0,0) band (cm^{-1}).

N	$P_1(N)$	$P_{12}(N)$	$P_2(N)$	$Q_1(N)$	$Q_{12}(N)$	$Q_2(N)$	$R_1(N)$	$R_2(N)$	$R_{21}(N)$
0							3920.789(−3)		
2				3918.076(0)			3928.904(3)	3947.808(−9)	
4				3918.524(2)		3935.543(0)	3935.619(5)	3951.017(−1)	3951.000(2)
6	3897.378(4)		3912.784(−3)	3917.650(1)		3931.639(−7)	3941.073(1)	3953.880(0)	3953.856(4)
8	3888.939(−1)	3888.972(−4)				3927.352(4)		3956.263(−4)	3956.229(−2)
10	3879.384(3)	3879.424(−2)	3890.259(0)	3912.466(0)	3912.509(−2)	3922.523(−5)	3948.682(6)	3958.075(0)	3958.032(2)
12	3868.794(6)	3868.840(−1)	3878.202(7)	3908.331(−3)			3950.972(2)	3959.229(1)	3959.175(1)
14			3965.485(−6)	3903.255(4)		3911.002(5)	3952.316(−5)	3959.679(3)	
16				3897.252(0)			3952.750(−6)	3959.382(−3)	
18				3890.367(3)		3896.640(6)	3952.289(−7)	3958.331(1)	
20	3817.088(−4)			3882.604(1)		3888.326(0)	3950.952(−3)	3956.491(−3)	
22						3879.251(4)	3948.745(1)		
24	3786.020(0)								
	$O_1(8)$ 3865.542(30)							$S_2(2)$ 3959.863(−10)	

$$\hat{H} = \hat{B}(r)(\mathbf{N}-\mathbf{L})^2 + \hat{A}(r)L_z S_z + \hat{A}'(r)(L_x S_x + L_y S_y) + \hat{\gamma}(r)\mathbf{N}\cdot\mathbf{S} \qquad (2)$$

in the unit of cm^{-1} where the first term represents the rotational energy, the second and third the spin–orbit interaction, and the fourth the spin–rotation interaction. **N**–**L**, **L**, and **S** are a dimensionless rotational angular momentum vector, an electronic orbital angular momentum, and an electron spin angular momentum vector, respectively. The total angular momentum is $\mathbf{J} = \mathbf{N} + \mathbf{S}$.

Three steps of contact transformation and averaging (Van Vleck transformation) brings the Hamiltonian of Eq. (2) into a rotational Hamiltonian applicable to the numerical analysis. They are: (1) contact transformation of electronic operators and averaging with electronic wave functions which introduces the p and q terms related to Λ doubling, (2) the vibrational contact transformation which introduces the centrifugal distortion, and (3) the spin–orbit–rotation contact transformation which eliminates the indeterminacy between the spin–rotation constant γ and the centrifugal constant for the spin–orbit interaction A_D. The resulting Hamiltonian is

$$H = B\mathbf{N}^2 - D\mathbf{N}^4 + H\mathbf{N}^6 + [(A + A_D\mathbf{N}^2), L_z S_z]_+/2 + \tfrac{1}{2}p(\Lambda_+^2 S_- N_- + \Lambda_-^2 S_+ N_+) - \tfrac{1}{2}q(\Lambda_+^2 N_-^2 + \Lambda_-^2 N_+^2), \qquad (3)$$

where $[\ \ ]_+$ indicates an anticommutator. We substitute $\mathbf{N} = \mathbf{J} - \mathbf{S}$ in Eq. (3) and calculate the matrix for the Hamiltonian using the matrix elements

$$\langle J,\Omega \pm 1|J_\mp|J,\Omega\rangle = [J(J+1) - \Omega(\Omega \pm 1)]^{1/2},$$
$$\langle S,\Sigma \pm 1|S_\pm|S,\Sigma\rangle = [S(S+1) - \Sigma(\Sigma \pm 1)]^{1/2}, \qquad (4)$$

and

$$\langle \Lambda = \pm 1|\Lambda_\pm^2|\Lambda = \mp 1\rangle = 1,$$

where $\Omega = \Lambda + \Sigma$ is the electronic angular momentum along the molecular axis. The basis functions of Hund's case (a) $|JS\Omega\Sigma\Lambda\rangle$ are used. (J_-, S_+, and Λ_+) and (J_+, S_-, and Λ_-) are the raising and the lowering operators for Ω, Σ, and Λ, respectively. The $\Lambda \pm$ operators resulted from the electronic contact transformation in which raising and lowering of Λ is retained using the Eckart–Wigner theorem.

For each value of J, we have two nearly degenerate 2×2 matrices between $^2\Pi_{u1/2}$ (for which $\Sigma = \mp 1/2$, $\Lambda = \pm 1$, and $\Omega = \pm 1/2$) and $^2\Pi_{u3/2}$ (for which $\Sigma = \pm 1/2$, $\Lambda = \pm 1$, and $\Omega = \pm 3/2$). The diagonal elements of the $^2\Pi_{u1/2}$ and the $^2\Pi_{u3/2}$ states are

$$B(x^2+1) - D(x^4+3x^2) + H(x^6+6x^4+x^2) - \frac{1}{2}[A + A_D(x^2+1)] \pm \left(\frac{p}{2}+q\right)x \qquad (5)$$

and

TABLE II. Transition frequencies of C_2^- (1,1) band (cm^{-1}).

N	$Q_1(N)$	$Q_{12}(N)$	$Q_2(N)$	$Q_{21}(N)$	$R_1(N)$	$R_2(N)$
2	3805.047(−2)		3826.139(−3)			
4			3822.524(0)		3822.418(−2)	
6	3804.625(0)	3804.656(6)			3827.823(0)	
8			3814.367(3)	3814.330(−1)		
10			3809.562(0)			3844.755(0)
12	3795.365(2)		3804.146(−6)			3845.866(2)
14	3790.303(−3)		3798.076(1)			3846.273(3)
16	3784.331(−5)		3791.292(3)			3845.936(−3)
18			3783.770(3)			

TABLE III. Transition frequencies of C_2^- (0,1) band (cm^{-1}).

N	$P_1(N)$	$P_2(N)$	$Q_1(N)$	$Q_2(N)$	$R_1(N)$	$R_2(N)$
6			2160.533(−2)	2174.521(−7)		
8	2132.316(−6)	2145.134(0)	2158.976(−2)	2170.721(−5)		2199.649(3)
10		2134.273(6)	2156.481(2)			2202.087(5)
12		2122.972(6)	2153.105(−6)	2161.870(2)		2204.006(7)
14			2148.925(−1)	2156.673(8)		2205.355(10)
16			2143.958(−6)			2206.087(−1)
18				2144.510(3)		2206.196(−7)
20				2137.493(−15)		2205.666(−10)
22					2199.403(17)	

$$B(x^2-1)-D(x^4-x^2)+H(x^6-x^2)+\frac{1}{2}[A+A_D(x^2-1)]\,,$$

respectively, and the off-diagonal element is

$$-(x^2-1)^{(1/2)}\left[B-2Dx^2+H(3x^4+x^2)+\frac{A_D}{4}\mp\frac{1}{2}qx\right], \tag{6}$$

where $x \equiv J+1/2$. Negligible constant terms are omitted for the D and H terms of Eqs. (5) and (6). The small terms $\pm(p/2+q)x$ and $\mp qx/2$ in the diagonal and off-diagonal matrix element, respectively, break the degeneracy of the $\pm$ levels (Λ doubling). Because of the nuclear spin statistics, only one component of the split level is allowed. For this reason the effect of Λ doubling appears as a staggering of spectral lines rather than as a splitting. C_2^- belongs to the "inverted" case,[6] i.e., $A<0$ and the energy of the $^2\Pi_{u1/2}$ levels are higher than the corresponding $^2\Pi_{u3/2}$ levels. For rotational levels with low J values, for which the difference of the diagonal elements $-A+2B(\sim 28.2\ cm^{-1})$ is much larger than the off-diagonal elements $B[(J+1/2)^2-1]^{1/2}$ ($B\sim 1.635\ cm^{-1}$), Hund's case (a) is a good approximation. For higher rotational levels the mixing between the $^2\Pi_{u3/2}$ and the $^2\Pi_{u1/2}$ wave functions becomes larger [through the $-2B\,\mathbf{J}\cdot\mathbf{S}$ interaction of the first term of Eq. (3)] and the eigenfunctions of the levels corresponding more closely to Hund's coupling case (b) (spin-uncoupling). By taking a limit $A\to 0$ and equating the resulting energy values to $BN(N+1)$, we note that the $^2\Pi_{u3/2}$ and the $^2\Pi_{u1/2}$ levels in Hund's case (a) connect to the $F_1(J=N+\frac{1}{2})$ and the $F_2(J=N-\frac{1}{2})$ levels, respectively, in Hund's case (b). The diagonal matrix elements given in Eq. (5) look somewhat different from those for traditional treatment[50]; in the present treatment the rotational term $B\Lambda^2$ is counted as part of the electronic term. The traditional formula can be obtained by using $J(J+1)-\Lambda^2$ for $J(J+1)$. While the formulas given in Eq. (5) are more consistent for the contact transformation procedure given in this paper, the difference is immaterial for the least-squares fitting.

For the $^2\Sigma_g^+$ ground electronic state, for which the Hund's case (b) holds, the rotational Hamiltonian is

$$H=B(r)\mathbf{N}^2+\gamma(r)\mathbf{N}\cdot\mathbf{S}\,, \tag{7}$$

where the second term represents spin–rotation interaction. After the vibrational contact transformation we have the well-known energy expression

$$E=BN(N+1)-DN^2(N+1)^2+HN^3(N+1)^3+E_{sr}\,, \tag{8}$$

where the spin–rotation energy E_{sr} is

$$E_{sr}=\frac{\gamma}{2}N \quad \text{and} \quad -\frac{\gamma}{2}(N+1) \tag{9}$$

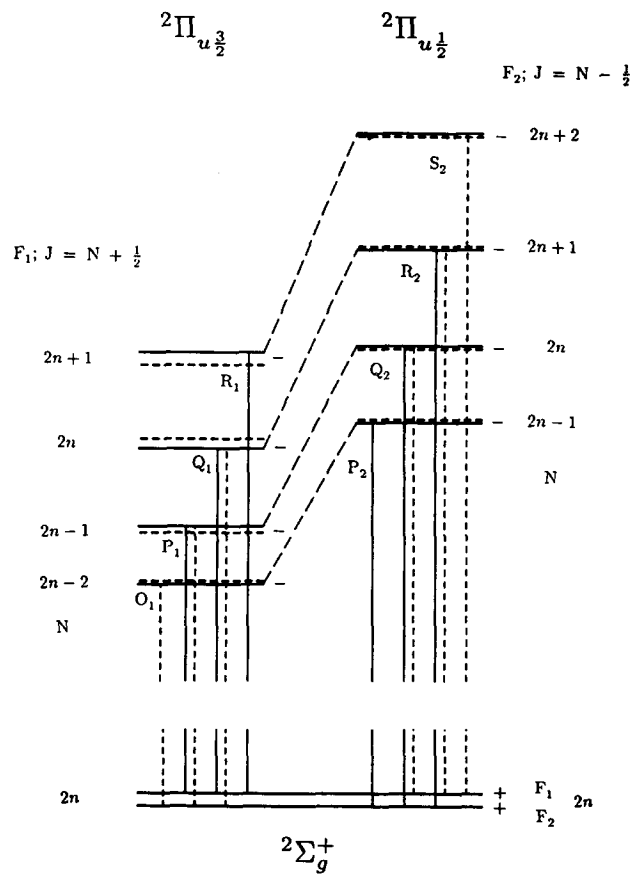

FIG. 5. Energy diagram of the $^2\Pi_u \leftarrow {}^2\Sigma_g^+$ electronic transition. Energy levels with broken lines are not allowed because of spin statistics. Solid vertical lines indicate fully allowed $F_1 \leftrightarrow F_1$ and $F_2 \leftrightarrow F_2$ transitions while broken vertical lines indicate weaker forbidden $F_1 \leftrightarrow F_2$ and $F_2 \leftrightarrow F_1$ transitions.

for the F_1 levels ($J = N + \frac{1}{2}$) and the F_2 levels ($J = N - \frac{1}{2}$), respectively.

A schematic energy level diagram for the two electronic states is given in Fig. 5, in which rotational energy levels, quantum numbers, and electron–rotation transitions are indicated. The symmetry of wave functions for an individual rovibronic state is specified by the $D_{\infty h}$ molecular symmetry group (or point group). The symmetry with respect to the space inversion E^* (which corresponds to σ_v of the point group), the 12 nuclear permutation (C_2), and the 12* permutation inversion operation (i) are specified by (+ , −), (s,a), and (g,u), respectively.[6] Since the ^{12}C nucleus is a boson with $I = 0$ we see from the character table that the symmetry of the total wave function has to be either Σ_g^+ (with + parity) or Σ_u^- (with − parity), the nuclear spin wave function Σ_g^+, and the rotational wave function Σ_g^+ for even N, and Σ_g^- for odd N.[6,54] Thus, for the ground electronic state with the Σ_g^+ symmetry, only N = even levels are allowed. For the excited state with the Π_u symmetry, the Λ doubling splits the doubly degenerate levels into a Σ_u^+ and Σ_u^- pair. Only the latter satisfies the allowed total symmetry and thus only the transition to one component of a Λ doublet is allowed. Overall, because of $I = 0$ for the carbon nucleus, only s levels are allowed and the symmetry $\pm$ and g,u are synonymous; all ground state levels are $g+$ and all excited state levels are $u-$. The symmetry of vibrational wave functions is always Σ_g^+ and the symmetry shown in Fig. 5 applies to all three vibrational bands.

The selection rules for the transitions are $+ \leftrightarrow -$ and $\Delta J = 0, \pm 1$. Since the effect of spin-uncoupling occurs for relatively low J values, Hund's case (b) F_1, F_2 notation is used to specify all observed transitions. Most of the observed strong lines are $\Delta J = \Delta N$ "allowed" transitions ($F_1 \leftrightarrow F_1$, $F_2 \leftrightarrow F_2$) and form the main P, Q, and R series. Weaker "forbidden" transitions ($F_2 \leftrightarrow F_1$) have also been observed and assigned. Most of them are the $\Delta J = \Delta N - 1$ Q and R branches and the $\Delta J = \Delta N + 1$ P and Q branches which appear as satellites to the stronger allowed transitions, but an isolated $\Delta J = \Delta N + 1$ S transition and an isolated $\Delta J = \Delta N - 1$ O transition have also been observed.

For low J levels, for which Hund's case (a) is a good approximation for the $^2\Pi_u$ state, the forbidden transitions have nearly equal intensities as allowed transitions (see Fig. 3), while for high J levels the former are much weaker than the latter. For very high J levels the intensities of the $J'N' \leftarrow JN$ transition are proportional to[55]

$$\begin{Bmatrix} N' & J' & 1/2 \\ J & N & 1 \end{Bmatrix}^2,$$

i.e., the intensities of the forbidden transitions are weaker than those of the allowed transitions by about $-1/2N^2$. We have clearly seen forbidden transitions for the $R_{21}(N)$ series and the $P_{12}(N)$ series up to $N = 12$ as listed in Table I. The splitting between the allowed and forbidden lines gave an accurate value of the spin–rotation interaction constant γ in the $X\,^2\Sigma_g^+$ ground state. The intensities of the forbidden transitions are much weaker for Q branch transitions because wave functions are mixed with the phase which reduces the dipole matrix element for Q branch lines.

V. MOLECULAR CONSTANTS

The observed 103 lines [57 lines for the (0,0) band, 21 lines for the (1,1) band, and 25 lines for the (0,1) band] have been fit simultaneously to Eqs. (3) and (7) using the expressions given in Eqs. (5), (6), (8), and (9). The standard deviation of the fitting was 0.0068 cm^{-1}. The observed minus calculated frequencies are shown in parentheses for each transition in Tables I–III. The values of sextic centrifugal distortion constants could not be meaningfully determined and they were neglected. The determined rotation–electronic constants for the four vibronic states are listed in Table IV. The errors given for each constant are three standard deviations. The value of A_D could not be determined independently for the two vibrational states and they are set equal for the two states.

TABLE IV. Determined molecular constants for C_2^- (in cm^{-1}).[a]

Band origins of $A\,^2\Pi_u(v') \leftarrow X\,^2\Sigma_g^+(v)$

(v',v)	
(0,0)	3928.6595(43) = T_0
(1,1)	3815.6264(77)
(0,1)	2170.8479(99)

Molecular constants

	$X\,^2\Sigma_g^+$		$A\,^2\Pi_u$	
	$v=0$	$v=1$	$v=0$	$v=1$
ν	1757.8098(136)		1644.7767(125)	
B	1.738 36(19)	1.721 86(23)	1.635 01(19)	1.619 02(25)
$D \times 10^6$	6.59(28)	6.96(38)	6.23(29)	6.72(52)
A			−24.983(8)	−24.940(12)
$A_D \times 10^5$			−7(8)[b]	−7(8)[b]
$p \times 10^4$			−9.86(35)	−10.18(63)
$q \times 10^4$			−4.42(2)	−4.28(56)
$\gamma \times 10^3$	4.25(56)	3.79(59)		

[a] The numbers in parentheses are 3σ.

[b] Assumed to be equal for the $v = 0$ and $v = 1$ states.

TABLE V. Equilibrium molecular constants of C_2^- (in cm^{-1}).

	This work	$A\,^2\Pi_u$ state MHSL (Ref. 22)	ZPB (Ref. 19)	RM (Ref. 21)
T_e	3985.83(50)	4064(91)	3250	3550[a]
ω_e	1666.4(10)	1656(20)	1653	1646
$\omega_e x_e$	10.80(26)	10.80(26)		11
B_e	1.643 05(334)	1.630(5)		1.619
α_B	0.016 01(44)	0.0152		
A_e	−25.009(15)	−24(1)		
α_A	−0.048(22)			
r_e	1.307 68(13)	1.313	1.318	1.318

$X\,^2\Sigma_g^+$ state

ω_e	1781.189(18)	$\omega_e x_e$	11.671 7(48)	$\omega_e y_e$	0.009 981 28
B_e	1.746 66(32)	α_e	0.016 51(46)	r_e	1.268 31(13)

[a] Converted from their value of 0.44 eV to wave number units.

Molecular constants listed in Table IV allow us to derive equilibrium molecular constants to be compared with theoretical predictions of Zeitz, Peyerimhoff, and Buenker[19] and of Rosmus and Werner.[21] The derived equilibrum constants are summarized in Table V together with the previous experimental results and theoretical predictions. In order to derive these constants the relations[6]

$$E_v = \omega_e(v+\tfrac{1}{2}) - \omega_e x_e(v+\tfrac{1}{2})^2 + \omega_e y_e(v+\tfrac{1}{2})^3 \quad (10)$$

and

$$B_v = B_e - \alpha_e(v+\tfrac{1}{2}), \quad (11)$$

have been used. Since we have band origins only for the $v = 1 \leftarrow 0$ transitions both in the X and the A electronic states, we used the $\omega_e x_e$ and $\omega_e y_e$ values of Mead *et al.*[22] which were determined from observation of high vibrational states. Since these higher order terms are small we can still arrive at values of ω_e and T_e with reasonable accuracy.

It is noted in Table V that the molecular constants of C_2^- for the $A\,^2\Pi_u$ state determined by Mead *et al.* are quite accurate and agree with our values to within their quoted uncertainties. The theoretical predictions by Zeitz, Peyerimhoff, and Buenker[19] and Rosmus and Werner[21] agree with the experimental values as far as the vibrational frequencies and molecular structure are concerned but differ significantly for the energy separation between the $A\,^2\Pi_u$ and the $X\,^2\Sigma_g^+$ states.

The equilibrium vibration–rotation constants listed in Table V enable us to calculate force constants of C_2^- using formulas[56]

$$f_2 = \omega_e$$

$$f_3 = -\left[\alpha_e + \frac{6B_e^2}{\omega_e}\right]\left[\frac{\omega_e^3}{2B_e^3}\right]^{1/2}, \quad (12)$$

and

$$f_4 = -16\omega_e x_e + \frac{5}{3}\cdot\frac{f_3}{\omega_e},$$

where f_2, f_3, and f_4 are force constants in the unit of cm^{-1} defined as

$$V/hc = \frac{1}{2}f_2 q^2 + \frac{1}{3!}f_3 q^3 + \frac{1}{4!}f_4 q^4 + \cdots \quad (13)$$

in terms of the dimensionless normal coordinate q. The force constants F_n in the usual units $mdyn/(Å)^{n-1}$ are obtained using the formula

$$F_n = hcf_n\left(2\pi\sqrt{\frac{c\mu\omega_e}{h}}\right)^n. \quad (14)$$

These force constants are listed in Table VI.

TABLE VI. Force constants for the $X\,^2\Sigma_g^+$ and the $A\,^2\Pi_u$ states of C_2^-.

	$X\,^2\Sigma_g^+$	$A\,^2\Pi_u$
f_2	1781.2 cm^{-1}	1666.4 cm^{-1}
f_3	−616.8 cm^{-1}	−587.6 cm^{-1}
f_4	169.2 cm^{-1}	172.6 cm^{-1}
F_2	11.215 mdyn/Å	9.817 mdyn/Å
F_3	−69.148 mdyn/Å^2	−59.613 mdyn/Å^2
F_4	337.80 mdyn/Å^3	301.50 mdyn/Å^3

The equilibrium bond length and the vibrational frequency of C_2^- in the $^2\Sigma^+$ and $^2\Pi$ states as well as the separation of the two states are compared with those of isoelectronic species CO^+, N_2^+, and CN in Table VII. It is noted

TABLE VII. Equilibrium bond lengths, vibrational frequencies, and the separation of the $A\,^2\Pi_u$ and the $X\,^2\Sigma_g^+$ states of species isoelectronic to C_2^-.

	r_e (Å)		ν_e (cm^{-1})		T_e (cm^{-1})
	$^2\Sigma_g^+$	$^2\Pi_u$	$^2\Sigma_g^+$	$^2\Pi_u$	
CO^+[a]	1.115 1_4	1.124 3_7	2214.2_4	1562.0_6	20 733.3
N_2^+	1.116 42	1.174 9	2207.00	1903.7_0	9 166.9_5
CN	1.171 8_2	1.233 3	2068.59	1812.5_6	9 245.28
C_2^-	1.268 31	1.307 68	1781.189	1666.4	3 985.83
BO	1.204 5	1.353 3	1885.69	1260.70	23 958.76
BeF	1.361 0	1.393 5			33 233.7

[a] Values for CO^+, N_2^+, CN, BO, and BeF have been quoted from Ref. 65.

that because of the smaller nuclear charge, the bond length of C_2^- is considerably larger and the vibrational frequency lower than corresponding values for other species. If we compare the bond length and the vibrational frequency of C_2^- for the ground state (1.268 31 Å and 1781.189 cm^{-1}, respectively) with those of C_2 (1.242 53 Å and 1854.71 cm^{-1}, respectively) we note the electron attached to C_2 in the $3\sigma_g$ orbital does not vary the bonding much and, if anything, it weakens the C–C bond. This bond insensitivity to the outermost electron is observed also for the isoelectronic pair of CN^+ and CN (r_e = 1.1729 vs 1.171 82 Å and ω_e = 2033.05 vs 2068.59 cm^{-1}). The small value of T_e for C_2^- compared to other species also indicates the insensitivity of the C–C bond to the state of the outermost electron.

The values of spin–orbit interaction constant A and the Λ doubling constants p and q for the isoelectronic species are listed in Table VIII. The spin–orbit interaction constant is the first order average of the electronic spin–orbit Hamiltonian

$$H_{so}^{(e)} = \frac{e\mu}{mc} \sum_i \mathbf{S}_i \cdot \left\{ \sum_\alpha Z_\alpha r_{i\alpha}^{-3} (\mathbf{r}_i - \mathbf{r}_\alpha) \times \mathbf{p}_i/2 - \sum_{j \neq i} r_{ij}^{-3} (\mathbf{r}_i - \mathbf{r}_j) \times (\mathbf{p}_i/2 - \mathbf{p}_j) \right\}, \quad (15)$$

where μ is the Bohr magneton, S_i,r_i, and p_i are the spin, the coordinate, and the momentum of the ith electron and $Z_\alpha e$ and r_α are the charge and the coordinate of the αth nuclei. $r_{i\alpha}$ and r_{ij} are the distance between the ith electron and the αth nucleus, and the distance between the ith and the jth electrons, respectively. The first term in Eq. (15) (the spin–orbit interaction) results from the interaction of the electron magnetic moment and the magnetic field which the electron "feels" moving in the nuclear electric field. The second term (the spin–other orbit interaction) arises from the interaction of the electron magnetic moment and the field resulting from the other electrons. The appearance of $\mathbf{p}_i/2$ instead of $\mathbf{p}_i$ results from the Thomas precession.[59] It has been shown that the first term gives a large negative value which is reduced by the smaller positive value due to the second term.[52] Since the first term is proportional to $1/r_{i\alpha}^3$, the lower value of A for C_2^- compared to other isoelectronic species is reasonable because the outermost electron is farther away from nuclei compared with other species.

The values of the Λ doubling constants p and q are poorly determined, yet they show some trend as we go down Table VIII. The value of q, which arises from the second-order perturbation treatment of the off-diagonal terms of L, is more or less constant, the value of p which arises from the coupling of the off-diagonal term of L and the spin–orbit interaction changes rather rapidly and even changes sign in C_2^-. The variation may be largely explained as due to the variation of the spin–orbit interaction discussed earlier. The drastic variation of the spacing between the $A\,^2\Pi_u$ and the $X\,^2\Sigma_g^+$ states do not affect these constants because the off-diagonal matrix elements do not exist between the *gerade* and *ungerade* states. *Ab initio* calculations of these constants are awaited.

TABLE VIII. Spin–orbit interaction constant A and Λ doubling constants p, q for species isoelectronic to C_2^- (in cm^{-1}).

	A_0	$p(\times 10^3)$	$q(\times 10^4)$
CO^+	−122.135(25)[a]	16.2(27)[a]	−3.0(18)[a]
N_2^+	−74.6[b]	4.84[b]	−6.0[b]
CN	−52.685[c]	8.42[c]	−3.89[c]
C_2^-	−24.985(8)	−0.99(4)	−4.42

[a] Reference 57.
[b] Reference 58.
[c] Reference 53.

VI. ASTROPHYSICAL IMPLICATIONS

The three diatomic species isoelectronic to C_2^- have all played important roles as astronomical probes. The $A\,^2\Pi \leftarrow X\,^2\Sigma^+$ transition of CO^+ was observed in a comet tail in 1907 by Deslandres[60] before it was identified as due to CO^+ in 1909 by Fowler.[61] The same transitions have also been observed for N_2^+ in the comet tail and for CN in the comet head.[62] The visible spectrum[63] and the millimeter wave spectrum[64] of CN have been an important probe for interstellar space. We believe that the visible spectrum observed by Herzberg and Lagerqvist[8] and the infrared spectrum reported in this paper will be a very useful astronomical probe in the near future.

The infrared $A\,^2\Pi_u \leftarrow X\,^2\Sigma_g^+$ transition of C_2^- is unique as an astronomical probe in two respects. First the carrier of the spectrum is a negative ion with only carbon nuclei. Thus, as suggested by Vardya and Krishna Swamy,[28] it may be observable in carbon stars. Compared with the H^- ion for which the electron affinity is only 0.75 eV, the C_2^- ion has much higher electron affinity of 3.4 eV and thus the bound–bound transitions are relatively much more important. While Wallerstein considered the electron attachment to C_2 to be the only production mechanism of C_2^-, our plasma chemistry experiment seems to show that there are a variety of ways to produce C_2^- by dissociative electron attachment starting from other molecules as in Eq. (1). Second, the $A\,^2\Pi_u \leftarrow X\,^2\Sigma_g^+$ transition is exceptional because the electronic transition appears in the infrared region. This means that we can observe the absorption spectrum of objects which have higher extinction and also the emission spectrum from relatively cool objects. The lifetime of spontaneous emission is given to be 49.9 μs by the *ab initio* calculations of Rosmus and Werner,[21] a very small value for an infrared transition because of the large transition dipole moment. The transitions reported in this paper are not complete because of atmospheric water interference, but we have complete calculated tables of all frequencies. The table is available on request from the last author.

ACKNOWLEDGMENTS

We wish to thank G. Herzberg and J. K. G. Watson for reading this paper. This work has been supported by NSF Grant No. PHY 84-08316. We also acknowledge the partial support of the Petroleum Research Foundation administered by the American Chemical Society.

[1]R. E. Honig, J. Chem. Phys. **22**, 126 (1954).
[2]L. von Trepka, Z. Naturforsch. Teil A **18**, 1295 (1963).
[3]R. Locht and J. Momigny, Chem. Phys. Lett. **6**, 273 (1970).
[4]D. Feldman, Z. Naturforsch. Teil A **25**, 621 (1970).
[5]P. L. Jones, R. D. Mead, B. F. Kohler, S. D. Rosner, and W. C. Lineberger, J. Chem. Phys. **73**, 4419 (1980).
[6]G. Herzberg, *Molecular Spectra and Molecular Structure. I. Diatomic Molecules* (Van Nostrand, New York, 1950).
[7]G. Herzberg, Science **177**, 123 (1972).
[8]G. Herzberg and A. Lagerqvist, Can. J. Phys. **46**, 2363 (1968).
[9]D. E. Milligan and M. E. Jacox, J. Chem. Phys. **51**, 1952 (1969).
[10]M. McCarty, Jr. and G. W. Robinson, J. Chim. Phys. **56**, 723 (1959).
[11]R. P. Frosch, J. Chem. Phys. **54**, 2660 (1971).
[12]V. E. Bondybey and J. W. Nibler, J. Chem. Phys. **56**, 4719 (1972).
[13]W. C. Lineberger and T. A. Patterson, Chem. Phys. Lett. **13**, 40 (1972).
[14]U. Hefter, R. D. Mead, P. A. Schulz, and W. C. Lineberger, Phys. Rev. A **28**, 1429 (1983).
[15]H. E. Popkie and W. H. Henneker, J. Chem. Phys. **55**, 617 (1971).
[16]P. W. Thulstrup and E. W. Thulstrup, Chem. Phys. Lett. **26**, 144 (1974).
[17]J. Barshun, J. Phys. B **7**, 155 (1974).
[18]P. E. Cade and A. C. Wahl, At. Data Nucl. Data Tables **13**, 339 (1974).
[19]M. Zeitz, S. D. Peyerimhoff, and R. J. Buenker, Chem. Phys. Lett. **64**, 243 (1979).
[20]H. Gollisch, J. Phys. B **14**, 4451 (1981).
[21]P. Rosmus and H. J. Werner, J. Chem. Phys. **80**, 5085 (1984).
[22]R. D. Mead, V. Hefter, P. A. Schulz, and W. C. Lineberger, J. Chem. Phys. **82**, 1723 (1985).
[23]R. Wildt, Astrophys. J. **89**, 295 (1939).
[24]S. Chandrasekhar, Rev. Mod. Phys. **16**, 301 (1944).
[25]L. M. Branscomb and B. E. J. Pagel, Mon. Not. R. Astron. Soc. **118**, 258 (1958).
[26]M. S. Vardya, Mem. R. Astron. Soc. **71**, 249 (1967).
[27]G. Wallerstein, Astron. Astrophys. **105**, 219 (1982).
[28]M. S. Vardya and K. S. Krishna Swamy, Chem. Phys. Lett. **73**, 616 (1980).
[29]M. W. Crofton, W. A. Kreiner, M.-F. Jagod, B. D. Rehfuss, and T. Oka, J. Chem. Phys. **83**, 3702 (1985).
[30]M. M. W. Crofton, M.-F. Jagod, B. D. Rehfuss, W. A. Kreiner, and T. Oka, J. Chem. Phys. **88**, 666 (1988).
[31]M. W. Crofton, M.-F. Jagod, B. D. Rehfuss, and T. Oka, J. Chem. Phys. **86**, 3755 (1987).
[32]A. Pine, J. Opt. Soc. Am. **64**, 1683 (1974).
[33]C. S. Gudeman, M. M. Begemann, J. Pfaff, and R. J. Saykally, Phys. Rev. Lett. **50**, 727 (1983).
[34]J. C. Owrutsky, N. H. Rosenbaum, L. M. Tack, and R. J. Saykally, J. Chem. Phys. **83**, 5338 (1985).
[35]D. J. Liu and T. Oka, J. Chem. Phys. **84**, 2426 (1986).
[36]N. H. Rosenbaum, J. C. Owrutsky, L. M. Tack, and R. J. Saykally, J. Chem. Phys. **84**, 5308 (1986).
[37]B. D. Rehfuss, M. W. Crofton, and T. Oka, J. Chem. Phys. **85**, 1785 (1986).
[38]K. Kawaguchi and E. Hirota, J. Chem. Phys. **84**, 2953 (1986).
[39]L. M. Tack, N. H. Rosenbaum, J. C. Owrutsky, and R. J. Saykally, J. Chem. Phys. **84**, 7056; **85**, 4222 (1986).
[40]M. Gruebele, M. Polak, and R. J. Saykally, J. Chem. Phys. **86**, 1698 (1987).
[41]M. Polak, M. Gruebele, and R. J. Saykally, J. Am. Chem. Soc. **109**, 2884 (1987).
[42]M. Gruebele, M. Polak, and R. J. Saykally, J. Chem. Phys. **86**, 6631 (1987).
[43]R. J. Saykally, Philos. Trans. R. Soc. London (in press).
[44]M. Greubele, M. Polak, and R. J. Saykally, J. Chem. Phys. **87**, 1448 (1987).
[45]W. Klebsch, K. Yamada, and G. Winnewisser, J. Mol. Spectrosc. **99**, 479 (1983).
[46]C. Amiot and G. Guelachvili, J. Mol. Spectrosc. **59**, 171 (1976).
[47]J.-M. Flaud, C. Camy-Peyret, and R. A. Toth, *Water Vapour Line Parameters from Microwave to Medium Infrared, International Tables of Selected Constants 19* (Pergamon, Oxford, 1981).
[48]E. Hill and J. H. Van Vleck, Phys. Rev. **32**, 250 (1928).
[49]R. S. Mulliken and A. Christy, Phys. Rev. **38**, 87 (1931).
[50]R. N. Zare, A. L. Schmeltekopf, W. J. Harrop, and D. L. Albritton, J. Mol. Spectrosc. **46**, 37 (1973).
[51]J. M. Brown and J. K. G. Watson, J. Mol. Spectrosc. **65**, 65 (1977).
[52]J. M. Brown, E. A. Colburn, J. K. G. Watson, and F. D. Wayne, J. Mol. Spectrosc. **74**, 294 (1979).
[53]A. J. Kotlar, R. W. Field, J. I. Steinfeld, and J. A. Coxon, J. Mol. Spectrosc. **80**, 86 (1980).
[54]P. R. Bunker and D. Papoušek, J. Mol. Spectrosc. **32**, 419 (1969).
[55]I. C. Bowater, J. M. Brown, and A. Carrington, Proc. R. Soc. London Ser. A **333**, 265 (1973).
[56]L. D. Landau and E. M. Lifshitz, *Quantum Mechanics* (Pergamon, Oxford, 1965).
[57]R. D. Brown, R. G. Dittman, and M. C. McGilvery, J. Mol. Spectrosc. **104**, 337 (1984).
[58]E. A. Colburn and A. E. Douglas, J. Mol. Spectrosc. **65**, 332 (1977).
[59]L. H. Thomas, Nature **117**, 514 (1926).
[60]H. Deslandres, C. R. Acad. Sci. (Paris) **145**, 445 (1907).
[61]A. Fowler, Mon. Not. R. Astron. Soc. **70**, 176 (1909).
[62]G. Herzberg, in *Highlights of Astronomy*, edited by P. A. Wayman (IAU, 1980), Vol. 5, p. 3.
[63]A. McKellar, Publ. Dom. Astrophys. Obs. Victoria B.C. **VII**, 251 (1941).
[64]A. A. Penzias, R. W. Wilson, and K. B. Jefferts, Phys. Rev. Lett. **32**, 701 (1974).
[65]K. P. Huber and G. Herzberg, *Constants of Diatomic Molecules* (Van Nostrand, New York, 1979).